Cybotactic behavior in the de Vries smectic-A^* liquid-crystal structure formed by a silicon-containing molecule

Seong Ho Ryu,[1] Tae Joo Shin,[2] Tao Gong,[3] Yongqiang Shen,[4] Eva Korblova,[3] Renfan Shao,[4] David M. Walba,[3]
Noel A. Clark,[4] and Dong Ki Yoon[1,*]

[1]*Graduate School of Nanoscience and Technology and KINC, KAIST, Daejeon, 305-701, Republic of Korea*
[2]*Pohang Accelerator Laboratory, POSTECH, Pohang, 790-784, Republic of Korea*
[3]*Department of Chemistry and Liquid Crystal Materials Research Center, University of Colorado, Boulder, Colorado 80309, USA*
[4]*Department of Physics and Liquid Crystal Materials Research Center, University of Colorado, Boulder, Colorado 80309, USA*

We have identified a metastable liquid-crystal (LC) structure in the de Vries smectic-A^* phase (de Vries Sm-A^*) formed by silicon-containing molecules under certain boundary conditions. The phase transition with the metastable structure was observed in a LC droplet placed on a planar aligned substrate and LCs confined in the groove of a silicon microchannel. During the rapid cooling step, a batonnet structure was generated as an intermediate and metastable state prior to the transition that yielded the thermodynamically stable toric focal conic domains. This distinctive behavior was characterized using depolarized reflection light microscopy and grazing incidence x-ray diffraction techniques. We concluded that the silicon groups in the molecules that formed the de Vries phase induced the formation of layered clusters called cybotactic structures. This observation is relevant to an exploration of the physical properties of cybotactic de Vries phases and gives a hint as to their optoelectronic applications.

PACS number(s): 61.30.Pq, 61.30.Cz, 61.30.Hn

I. INTRODUCTION

Smectic liquid-crystal (LC) phases tend to display layer shrinkage during the phase transition from the smectic-A (Sm-A) phase to the smectic-C (Sm-C) phase, yielding zigzag defects between the surface-stabilized cells [1–3]. Layer shrinkage degrades the optical properties of the LC and has precluded the use of smectic LCs in electro-optical devices [4,5]. de Vries LC phases are interesting in that they do not display layer shrinkage during their phase transitions [6], making them good candidates for realizing smectic LC-based electro-optical devices.

de Vries proposed a diffuse cone model in 1979 to explain the low levels of layer shrinkage in de Vries phases, in which the molecules were described as being tilted within a diffuse cone in the Sm-A phase [Fig. 1(c)] [7,8]. Under this model, only the tilt direction of the LC mesogenic units changes during the phase transition, even after the transition has ended at the Sm-C phase, and the layer spacing does not change. Since this model was proposed, a considerable number of studies have examined the physical properties of de Vries phases [9–17]. Although many LC researchers have focused on phase transitions in sandwiched glass cells, relatively few studies have examined the effects of the boundary conditions, such as confined geometries or hybrid boundaries composed of planar and homeotropic surfaces, in search of other exotic behaviors in the de Vries phases [Figs. 1(e) and 1(f)]. Topographic confinement was shown to be a useful tool for studying various LC phases [18,19]. For example, a silicon microchannel offers a simple tool for controlling the spatial organization of the LC phase, or even defect structures [19–21].

In this article, we discovered that a batonnet structure is formed as an intermediate and metastable state in a W599

LC droplet on a planar aligned surface during cooling from the isotropic to the de Vries Sm-A^* phase. In an effort to build an appropriate model to explain this distinctive behavior, we examined a de Vries LC having a tricarbosilane (TCS) tail group under topographic confinement conditions in a microchannel. *In situ* depolarized reflected light microscopy (DRLM) and grazing incidence x-ray diffraction (GIXD) results obtained during cooling revealed cybotactic behaviors that arose from the properties of the layered W599 clusters.

II. EXPERIMENT

Material. W599 was synthesized according to the following procedure (Fig. S1 in the Supplemental Material) [22,23]. A mixture of the mono- and dinitrated biphenol (1) was coupled to R-2-pentanol under Mitsunobu coupling conditions to give the desired nitrophenol ether. The TCS tail (6) was synthesized through a nucleophilic substitution reaction [24]. Commercially available chlorotrimethylsilane was successfully converted to the corresponding Grignard reagent, and reacted with chlorodimethylsilane via a substitution pathway to yield chlorodicarbosilane (5). A similar reaction was used to convert chlorodicarbosilane (5) to the Grignard reagent, followed by coupling with chlorodimethylsilane to generate the desired TCS tail (6). Hydrosilylation was then carried out between the TCS tail (6) and the alkene (7), which was easily generated under Williamson ether conditions in the presence of 6-bromo-1-hexene and benzyl 4-hydroxybenzoate, to achieve compound (8). Compound (8) was then deprotected via catalytic hydrogenation to afford the carboxylic acid (9), which was directly coupled with the nitrophenol ether (4) under dicyclohexylcarbodiimide (DCC) coupling conditions to provide W599 (10).

Sample preparation. Microchannels were fabricated on a (100) Si wafer using photolithography and reactive ion etching

---
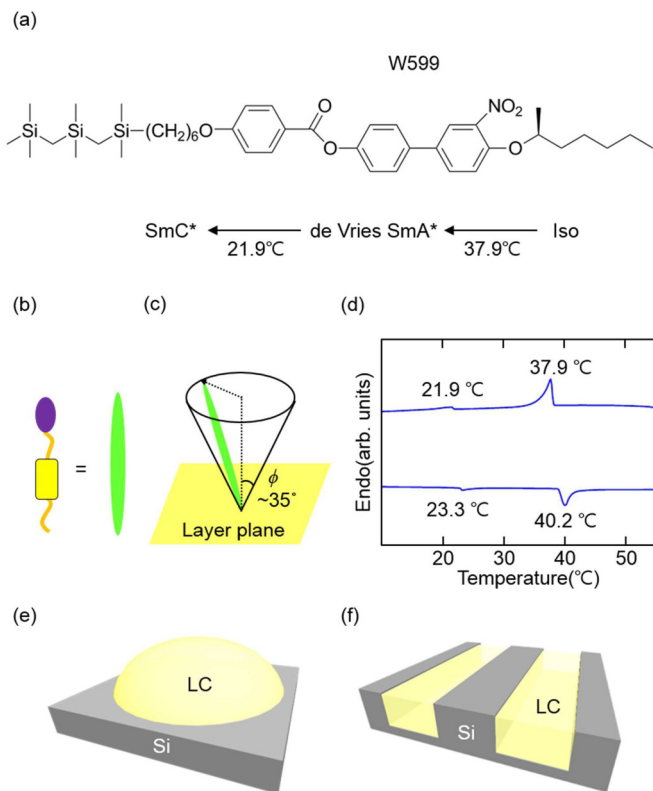
FIG. 1. (Color online) The molecule used (W599) and the experimental setup. (a) Molecular structure of W599 and its thermal phase transitions upon cooling. (b) A molecular model based on the volume of each atom of the molecule. In this model, the purple (ellipse), yellow (rectangle), and orange (coil) parts correspond to the tricarbosilane (TCS) group, aromatic rigid core, and aliphatic parts, respectively. This model is simplified to a single rod, shown in green, and (c) positioning of the rod in the diffused cone between smectic layers. The green rod has a specific tilt angle ($\phi \sim 35°$) with respect to the layer plane. (d) DSC thermogram measured at a rate of 5 °C min^{-1} during the first cooling and second heating to determine the thermal phase transitions of W599. (e), (f) Schematic representations of a LC droplet on a silicon substrate and LCs in silicon microchannels.

techniques. The microchannels were 5 μm in depth, 5 μm in width, and 10 mm in length. Organic residues were removed by chemically cleaning the microchannels by ultrasonication in acetone, followed by rinsing several times with ethanol and de-ionized water. The microchannels were filled with the sample by capillary action. A sample was placed at the microchannel opening, and the system was heated above 40 °C (corresponding to the isotropic phase) using a heating stage with a temperature controller (Linkam LTS350 and TMS94). The sample was then cooled to 33 °C (corresponding to the de Vries Sm-A^* phase). Cooling and heating cycles were repeated at different ramping rates during the subsequent DRLM observations.

Characterization. The samples were thermally analyzed by differential scanning calorimetry (DSC) (TA Instrument Q1000 v9.9). For this, the samples were heated and cooled at a rate of 5 °C min^{-1}, and N$_2$ purging was applied at a rate of 50 mL min^{-1}. Optical anisotropy measurements using cross polarizers under DRLM (Nikon LV100POL) revealed the

sample morphologies during the phase transition. The phase transition behaviors of the W599 in the silicon microchannel were controlled by varying the cooling rate between 0.1 and 30 °C min^{-1} to achieve slow cooling and rapid cooling, respectively. GIXD experiments were carried out at the 9A beamline of the Pohang Accelerator Laboratory (PAL). The size of the focused beam was $\sim$70 (V) $\times$ 450 (H) μm^2, and the energy was 11 keV. The sample-to-detector distance was fixed at 257 mm to investigate the small-angle scattering profile as well as the wide-angle scattering profile. The diffraction patterns were recorded using a two-dimensional charge-coupled-device (2D CCD) detector (Rayonix SX165, USA).

III. RESULTS

The molecule used in this experiment, W599, can be subdivided into three segments, as illustrated in Figs. 1(a) and 1(b): an aromatic rigid core (yellow), a TCS tail group (purple), and an aliphatic group (orange) [22]. In terms of LC formation, the most important part of the W599 molecule is the TCS tail group, in which the silicon atoms preferentially orient in a staggered conformation so as to reduce the steric hindrance between the methyl groups covalently bound to the silicon atoms [10,25–27]. The conformational energy is minimized by the TCS group's adoption of a spherical shape. The TCS group is more bulky than the aromatic rigid core or the aliphatic group [Fig. 1(b)]. Despite having an asymmetric shape, the molecule can be modeled as a rod that is able to freely rotate within a diffuse cone, thereby allowing a correspondence to a de Vries LC phase with a specific tilting angle ($\phi \sim 35°$) with respect to the layer plane [Fig. 1(c)]. Each molecule can freely rotate within its diffuse cone. The molecule-level degrees of orientational freedom create similarities between the de Vries phase and a Sm-A phase with a layered structure and without positional order. A phase transition from de Vries Sm-A^* to Sm-C^* is associated with the assumption of a single tilt angle (ϕ) by all molecules in a layer, such that the molecular arrangements resemble those of a normal Sm-C phase.

Differential scanning calorimetry (DSC) was used to characterize W599 during cooling and subsequent heating, and the resulting diagrams are shown in Fig. 1(d). Cooling at a rate of 5 °C min^{-1} induced major exothermic transitions at 37.9 and 21.9 °C, which corresponded to mesophase transitions, respectively, in the de Vries Sm-A^* phase and Sm-C^* phase. The subsequent heating scan revealed endothermic transitions at 23.3 and 40.2 °C.

Hydrophilic surfaces were prepared to induce planar alignment among the LC molecules by thoroughly cleaning a flat single-crystal Si substrate (100 orientation) to remove organic and inorganic impurities by ultrasonication in acetone. The substrate was then rinsed several times with ethanol and de-ionized water. A viscous W599 sample droplet was placed on the substrate and heated to form an isotropic phase that spread the sample across the treated silicon substrate [Fig. 1(e)].

The nucleation and growth of optical textures in the de Vries phases were investigated by DRLM during cooling from an isotropic state at a rate of 10 °C min^{-1}. The transition temperature measured here differed slightly relative to the

value obtained from the DSC results because the sample was open to air at room temperature (Fig. 2). It should be noted that under these experimental conditions, the phase transition occurred even if the ramping had been stopped at the nucleation stage (∼40 °C). The TFCDs then formed directly without passing through an intermediate state. Thus, rapid cooling at a rate of 10 °C min^{-1} was applied to generate the relatively unstable batonnet structures [28]. Nucleation and growth of the batonnet structures and TFCDs in the de Vries Sm-A^* phase displayed the following typical characteristics: (1) Scattered small batonnet structures formed from an isotropic phase [Fig. 2(a)]. (2) The number of distinct batonnet structures increased but these structures did not coalesce into a large domain under the rapid cooling conditions [Fig. 2(b)]. (3) TFCDs formed from the batonnet domains [Fig. 2(c)] [29,30]. (4) Finally, most of the batonnet domains converted to TFCDs. The magnified image shown in Fig. 2(d) reveals Maltese cross patterns that resulted from the projection of the radial director field of the mesogenic units onto the substrate [31]. The identical tendency was found in another de Vries LC (Fig. S2 in the Supplemental Material) [23].

In general, LC molecules in a smectic LC droplet on a planar aligned silicon wafer tend to align parallel to the substrate, whereas those near an LC-air boundary tend to align perpendicular to the air interface. The batonnet structures in a smectic phase are mainly found in a sample prepared between planar aligned substrates (Fig. S3 in the Supplemental Material) [23]. By contrast, our DRLM studies of the de Vries phase formed from a molecule having a TCS group revealed that batonnet structures formed under hybrid boundary conditions comprising a planar silicon substrate and an LC-air interface.
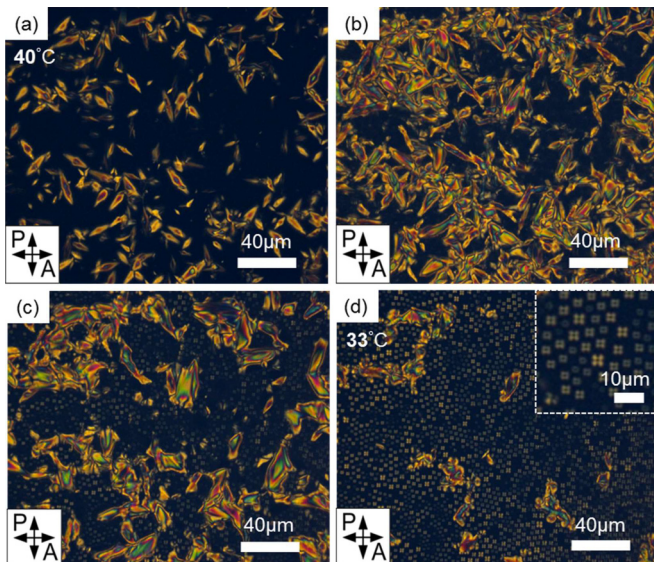
FIG. 2. (Color online) DRLM images of a W599 droplet on a Si substrate, collected under crossed polarizers upon cooling from an isotropic phase in the bulk state. (a) Nucleation and growth of the batonnet structures were observed around 40 °C; (b) the batonnet structures filled in most of the droplet. (c) The batonnet-to-TFCD transition proceeded slowly. (d) Finally, the entire droplet became filled with TFCDs at 33 °C. Inset: An enlarged image shows Maltese cross patterns typically found in TFCDs [19].

These results suggested that the assembly or aggregation of LC molecules might occur prior to surface anchoring under the competing influences of the hydrophilic substrate and hydrophobic air boundary conditions. This competition affected the formation of smectic layered structures during the early stages of an isotropic phase-to-de Vries Sm-A^* transition, with the thermodynamically stable TFCDs appearing only at the end of the phase transition. Sequential changes in the optical properties of the LC during cooling suggested that the batonnet structures were metastable and reassembled to form TFCDs at the end of the transition. Although the system passed through a local free energy minimum corresponding to the batonnet structure during the transition to the de Vries Sm-A^* phase, the energetically stable structure was found to be the TFCD, which constituted a global free energy minimum.

The observation of birefringence in the interconnecting areas of the bright Maltese cross patterns in the DRLM measurements yielded information about the normal Sm-A and de Vries phases. In a normal Sm-A phase, retardation is not typically produced in these regions under cross polarizers because the interconnecting molecules are perpendicularly aligned relative to the air interface, whereas the molecules in Maltese cross patterns are tangentially aligned. In the de Vries Sm-A^* phase, on the other hand, weak retardation was observed, even among the Maltese cross patterns, possibly due to the tilting of molecules within diffuse cones in the layers, as shown in the schematic diagram of Fig. 1(c).

We further explored the aggregation behavior in the de Vries Sm-A^* phase by confining the sample in a silicon microchannel. The microchannels, formed by rectangular grooves of width $w = 5$ μm, separation $s = 5$ μm, depth $d = 5$ μm, and length $L = 10$ mm, were prepared on the surfaces of single-crystal Si substrates (100 orientation) using conventional fabrication techniques that included photolithographic masking and reactive ion etching processes [Fig. 1(f)] [19]. The microchannels were then cleaned to provide planar anchoring surfaces, as described above. The microchannels were then filled with W599 by placing a sample droplet at the channel opening and heated to an isotropic melt stage. The melted sample then filled the microchannel under capillary action. All samples were prepared under open-air conditions to introduce a hydrophobic air boundary.

The formation of batonnet or TFCD structures could be controlled by modulating the sample cooling rate. Rapid or slow cooling rates induced the formation of, respectively, batonnet or TFCD structures. Rapid cooling at a rate of 30 °C min^{-1} induced a phase transition in the microchannels that resembled the transition observed in the LC droplet experiments (Fig. 2). Nucleation and growth of the batonnet structures were observed, although imperfect TFCDs formed in the channels [Figs. 3(a)–3(c)]. The channel and bulk droplet samples did differ in terms of the batonnet structure size. The microchannels did not allow the batonnet structures to grow as large as they did in the droplet sample. Rapid cooling also played an important role in freezing the unstable batonnet structures, which then induced the formation of irregular TFCDs at the end of the transition [Fig. 3(c)]. On the other hand, slow cooling at a rate of 0.1 °C min^{-1} resulted in the formation of excellent TFCDs in the channel. The
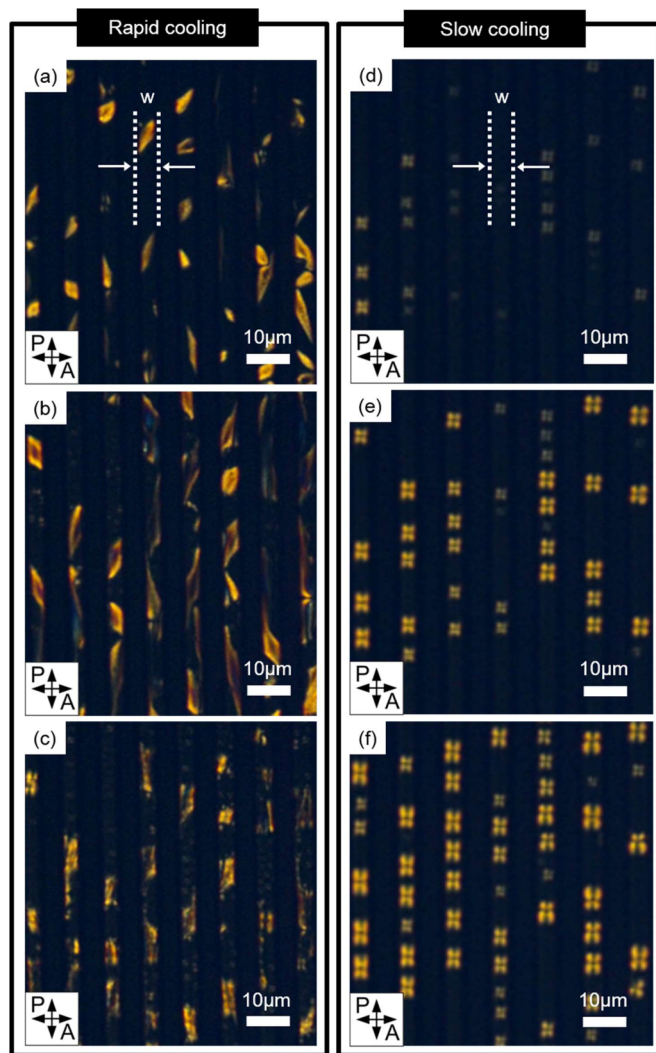
FIG. 3. (Color online) DRLM images of W599 in silicon microchannels (w, s, and $d = 5$ μm), prepared with rapid or slow cooling. All images were collected at a single position in the sample. (a)–(c) The behavior resembled the behavior observed in Fig. 2 during rapid cooling. (d)–(f) TFCDs formed directly without the generation of batonnet structures during slow cooling.

FIG. 4. (Color online) Schematic diagram showing the grazing incidence x-ray diffraction (GIXD) experimental setup and the obtained GIXD patterns. (a) The x-ray beam entered along the y axis of the microchannel, and the incident angle (θ) of the x-ray beam was 0.1°. 2D GIXD patterns collected at (b) 40 °C, (c) 39.1 °C, and (d) 33 °C. Enlarged views of the small-angle regions are shown to elucidate the layer orientations.

metastable batonnet structures were not observed under these experimental conditions [Figs. 3(d)–3(f)]. Taken together, these results indicate that the batonnet structures that form under the microchannel boundary conditions comprise a metastable state [32]. Deep gray regions between the TFCDs indicated a high-contrast birefringence difference with the silicon ridges of the microchannel, as observed in the LC droplet experiment. The TFCDs that formed in the W599 de Vries Sm-A^* phase were generated very slowly, in contrast to what has been observed in the formation of normal TFCDs in a Sm-A phase. Alkyl or semifluorinated rod-type molecules form very regular TFCDs, even under sample quenching conditions (Fig. S4 in the Supplemental Material) [19,23], indicating that the molecular reorganization proceeds very rapidly. These observations raise the following question: Which part of the W599 molecule most strongly affects the formation of a smectic phase? We examined the role of the

silicon group in W599, the TCS group, which tends to favor self-aggregation among molecules.

The phase transition behavior was examined at the molecular level. GIXD experiments were conducted using a synchrotron source at the 9A beamline of the Pohang Accelerator Laboratory (PAL). GIXD patterns [Fig. 4(a)] revealed the in-plane (q_x) and out-of-plane (q_z) inter- and intramolecular structures from measurements conducted at a grazing incident angle (θ) relative to the substrate [33]. An appropriate sample-to-detector distance (257 mm) was chosen to measure both the small-angle regions, which characterized the layer structures, and the wide-angle regions, which characterized the short-range molecular ordering within the layers. In general, q_{min}–q_{max} is defined by the experimental setup and is usually fixed by geometric limitations, such as the sample-to-detector distance and the detector size. Sequential two-dimensional (2D) GIXD patterns were obtained as the sample was cooled and transformed from the isotropic to the de Vries Sm-A^* phase. Three representative GIXD patterns at 40 °C (isotropic phase), 39.1 °C (the initial stage in the de Vries Sm-A^* phase), and 33 °C (the final stage in the de Vries Sm-A^* phase) are shown in Fig. 4 to characterize the phase transitions of the de Vries phase. Enlarged views of the small-angle regions clearly reveal the 2D orientational changes in the layer structures of the de Vries Sm-A^* phase.

A diffuse arc in the small-angle region was observed at the isotropic temperature [Fig. 4(b)], indicating that randomly oriented structures were present in the isotropic state. At 39.1 °C, corresponding to the beginning of the phase transition, a relatively bright center line ($\chi \sim 90°$) was observed in the diffraction pattern [Fig. 4(c)], indicating the presence of a structure aligned parallel to the microchannel axis. After the

transition to the de Vries Sm-A^* phase at 33 °C, the center line displayed very strong first- and second-order peaks, suggesting that highly ordered smectic layers had formed. These results were consistent with the DRLM images. The LC sample prepared by slow and rapid cooling showed an identical diffraction pattern, which indicates that the final layered structure is internally the same regardless of cooling rate (Fig. S5 in the Supplemental Material) [23]. A diffuse halo in the wide-angle region above this temperature changed to a more ordered symmetric pattern, which is discussed more extensively in Fig. 6.

The layer d spacing and intermolecular distances were quantitatively characterized by analyzing the q_z values from the GIXD patterns at $\chi = 90°$. The averaged intensities are plotted as a function of q_z over the small-angle region 0.10 Å$^{-1} < q_z < 0.20$ Å^{-1} at 33 °C in the de Vries Sm-A^* phase and coherence lengths are estimated by analysis of the full width at half maximum (FWHM) of the intensities at 40 and 39.5 °C (isotropic phase), 39.1 °C (the initial stage in the de Vries Sm-A^* phase), 36 °C (the middle stage in the de Vries Sm-A^* phase), and 33 °C (the final stage in the de Vries Sm-A^* phase) (Fig. 5). In the opened sample, the isotropic-to-de Vries Sm-A^* phase transition occurred at

40 °C, as shown in Fig. 2, because the air interface influenced the phase transition. At 33 °C, a very high intensity peak was found at $q_z \sim 0.175$ Å^{-1} ($d \sim 3.6$ nm) [Fig. 5(a)]. This peak position was exactly the same as the peak position observed in the bulk sample (Fig. S6 in the Supplemental Material) [23,34]. The change in coherence lengths was followed by two distinct stages at 39.1 °C [Fig. 5(b)]: (1) In the beginning of the phase transition from 40 to 39.1 °C (yellow part), the coherence length increased from 75 Å at 40 °C to 218 Å at 39.1 °C. (2) In the de Vries Sm-A^* phase from 39.1 and 33 °C (green part), there was no significant difference in the coherence length, which ranged from 218 to 195 Å.

This trend in the small-angle diffraction patterns and the change in coherence length obtained during the transition from the isotropic phase to the de Vries Sm-A^* phase support a model for the development of layer-clustered structures. The increased value of the coherence length to ~200 Å that shows correlation among smectic layers suggests that the layer-clustered structures are grown, and a single strong peak in the de Vries Sm-A^* phase indicates the presence of a very well-ordered layer structure having a specific layer spacing of 3.6 nm, in which the intensity is increased from 1 to 25 000, as illustrated in Fig. 7.

Further evidence of this behavior can be found from the intermolecular packing structure profiles derived from the wide-angle regions 0.8 Å$^{-1} < q_z < 1.6$ Å^{-1} (Fig. 6), measured at 33 °C, corresponding to the de Vries Sm-A^*
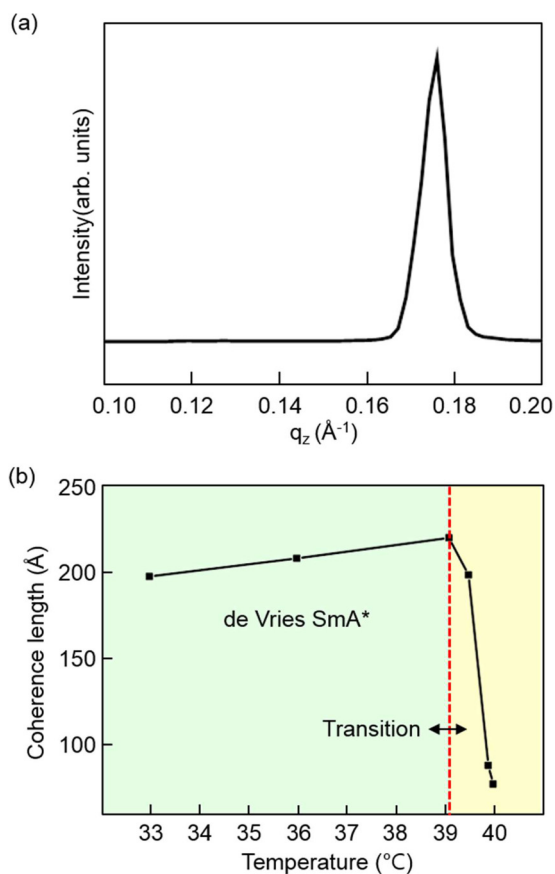
FIG. 5. (Color online) GIXD analysis in the small-angle region during a phase transition between the isotropic and de Vries Sm-A^* phases. (a) Intensity vs q plots in the de Vries Sm-A^* phase at 33 °C. (b) Coherence length vs temperature during the phase transition from 40 to 33 °C.
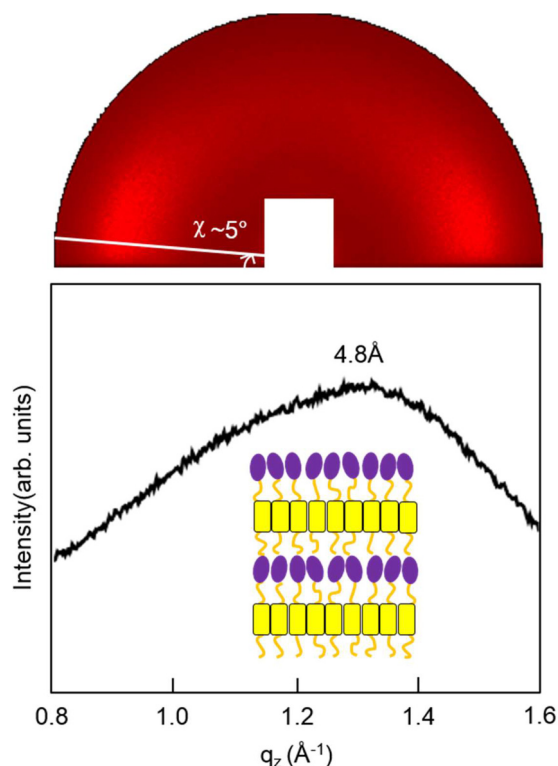
FIG. 6. (Color online) GIXD patterns in the wide-angle region, and 1D graphs at 33 °C as a function of the specific $\chi = 5°$. The 1D graph indicates the d spacing and the intermolecular packing of the aromatic rigid core and aliphatic group.

phase. In this region, the q value represents the intermolecular arrangement of W599 molecules for a specific χ. A maximum of peak was observed at $q_z \sim 1.31$ Å^{-1} ($\chi \sim 5°$), indicating an intermolecular distance of 4.8 Å, which corresponds to the distance between the neighboring aromatic cores and aliphatic groups aligned perpendicular to the bottom substrate of the microchannel. As shown in GIXD patterns of a wide-angle region [Figs. 4(d) and 6], a wide-angle peak was relatively broad ($0° < \chi < 40°$) and diffused, which is consistent with the circularly plotted one-dimensional (1D) graph for the isotropic phase at 40 °C and the de Vries Sm-A^* phase at 33 °C (Fig. S7 in the Supplemental Material) [23]. This diffused arc results from randomly oriented LC molecules having a specific tilting angle ($\sim 35°$) with the layer plane [Fig. 1(c)]. The wide-angle peak at $q_z \sim 1.1$ Å^{-1} representing intermolecular stacks of carbosilane moieties would appear if TCS groups of W599 molecules are assembled very well. However, bulky silicon-containing groups may be stacked horizontally in a layer and randomly separated by a range of distances in a smectic layer, as shown in the schematic sketch (Fig. 6) [35]. The W599 molecules may form layer structures with a horizontal alignment, but slightly random, in the microchannels, as shown in Fig. 6.

Based on the microscopy and diffraction results, the intramolecular and intermolecular structures formed during the phase transition from the isotropic to the de Vries Sm-A^* phase can be described as shown in Fig. 7. Weak diffuse peaks were observed in the small-angle region, even in the isotropic state, due to the presence of aggregated molecules [Fig. 4(b)]. This is consistent with the estimated coherence length (75 Å) in the small-angle region [Fig. 5(b)], showing that W599 molecules displayed characteristics that resembled a cybotactic phase having randomly oriented smecticlike clusters as a result of molecular aggregation [36–38]. Despite the observation of very weak birefringence in the DRLM images in this isotropic region [Figs. 2(a), 3(a), and 3(d)], the

GIXD results corroborate the characterization of a cybotactic nematiclike phase that has been found in the silicon- or fluorine-containing molecules [Fig. 7(a)] [39]. During the phase transition, the smecticlike clusters appeared to merge and form more ordered structures with an increased coherence length from 75 to 218 Å [Fig. 5(b)]. These structures appeared to be the batonnet structures observed in the DRLM images. The results suggested the presence of a cybotactic Sm-A phase due to the strong peak intensity observed in the center line ($\chi \sim 90°$) of the diffraction pattern at 39.1 °C [Fig. 4(c)]. The center-line peak indicated that the combined clusters have, on average, smecticlike layer structures [Figs. 5(c) and 7(b)]. A highly ordered layer structure was observed in the de Vries Sm-A^* phase as the TFCDs were generated by the densely packed smecticlike clusters, where the aromatic rigid cores (yellow) are closely packed by a π-π interaction while the aliphatic groups and TCS tail groups are randomly stacked (orange and purple), which results from randomly tilted W599 molecules in smectic layers. This transition was accompanied by the convergence of the weak and diffuse halolike GIXD peaks in the small-angle region into a single strong peak at 3.6 nm [Figs. 4(d), 5(a), and 7(c)]. Distinct intermolecular packing of each segment of the W599 molecule in the microchannels supports this model.

IV. CONCLUSION

In summary, we identified a metastable de Vries LC phase with a batonnet morphology based on DRLM observations. This batonnet morphology transitioned to a thermodynamically stable TFCD in both a LC droplet on a planar aligned silicon wafer and in a LC confined in a microchannel. These transitions were explored by varying the cooling rate from 0.1 to 30 °C min^{-1} in the silicon microchannels: (1) During rapid cooling, batonnet structures formed as an intermediate state, although the structure further evolved to yield irregular optical properties. (2) Slow cooling resulted in the formation of regular TFCDs without passing through a metastable state. Subsequent GIXD experiments hinted at a model for these observations, in which the silicon moieties of W599 affect the organization of the layered clusters. Highly ordered smectic layer structures with a d spacing of 3.6 nm were constructed. The DRLM images of these samples indicated the presence of TFCDs. This article, which has dealt with de Vries Sm-A^* phases having cybotactic clusters, advances our understanding of the molecular mechanisms underlying the physical properties of de Vries phases formed by LC molecules having silicon groups. Such LC phases are potentially applicable to the development of optoelectronic devices.
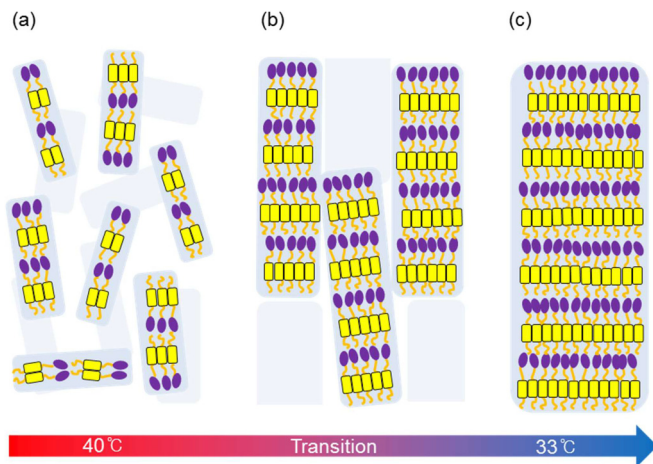
FIG. 7. (Color online) Schematic diagram of the molecular arrangements in (a) the isotropic but cybotactic nematiclike phase, (b) the transition state–cybotactic smectic phase, and (c) the de Vries Sm-A^* phase.

[1] N. A. Clark and S. T. Lagerwall, Appl. Phys. Lett. **36**, 899 (1980).

[2] T. P. Rieker, N. A. Clark, G. S. Smith, D. S. Parmar, E. B. Sirota, and C. R. Safinya, Phys. Rev. Lett. **59**, 2658 (1987).

[3] N. A. Clark and T. P. Rieker, Phys. Rev. A **37**, 1053 (1988).

[4] Y. Ouchi, H. Takezoe, and A. Fukuda, Jpn. J. Appl. Phys. **26**, 1 (1987).

[5] J. P. F. Lagerwall and F. Giesselmann, ChemPhysChem **7**, 20 (2006).

[6] A. de Vries, Mol. Cryst. Liq. Cryst. **41**, 27 (1977).

[7] A. de Vries, Mol. Cryst. Liq. Cryst. **49**, 143 (1979).

[8] A. de Vries, Mol. Cryst. Liq. Cryst. **49**, 179 (1979).

[9] Y. P. Panarin, V. Panov, O. E. Kalinovskaya, and J. K. Vij, J. Chem. Mater. **9**, 2967 (1999).

[10] M. S. Spector, P. A. Heiney, J. Naciri, B. T. Weslowski, D. B. Holt, and R. Shashidhar, Phys. Rev. E **61**, 1579 (2000).

[11] J. P. F. Lagerwall, F. Giesselmann, and M. D. Radcliffe, Phys. Rev. E **66**, 031703 (2002).

[12] K. L. Sandhyal, Y. P. Panarin, V. P. Panov, J. K. Vij, and R. Dabrowski, Eur. Phys. J. E **27**, 397 (2008).

[13] J. C. Roberts, N. Kapernaum, Q. Song, D. Nonnenmacher, K. Ayub, F. Giesselmann, and R. P. Lemieux, J. Am. Chem. Soc. **132**, 364 (2010).

[14] R. Korlacki, V. P. Panov, A. Fukuda, J. K. Vij, C. M. Spillmann, and J. Naciri, Phys. Rev. E **82**, 031702 (2010).

[15] J. Fernsler, D. Wicks, D. Staines, A. Havens, and N. Paszek, Liq. Cryst. **39**, 1204 (2012).

[16] Q. Song, D. Nonnenmacher, F. Giesselmann, and R. P. Lemieux, J. Mater. Chem. C **1**, 343 (2013).

[17] N. Hayashi, T. Kato, A. Fukuda, J. K. Vij, Y. P. Panarin, J. Naciri, R. Shashidhar, S. Kawada, and S. Kondoh, Phys. Rev. E **71**, 041705 (2005).

[18] H. Kim, Y. H. Kim, S. Lee, D. M. Walba, N. A. Clark, S. B. Lee, and D. K. Yoon, Liq. Cryst. **41**, 328 (2014).

[19] D. K. Yoon, M. C. Choi, Y. H. Kim, M. W. Kim, O. D. Lavrentovich, and H.-T. Jung, Nat. Mater. **6**, 866 (2007).

[20] D. K. Yoon, R. Deb, D. Chen, E. Korblova, R. Shao, K. Ishikawa, N. V. S. Rao, D. M. Walba, I. I. Smalyukh, and N. A. Clark, Proc. Natl. Acad. Sci. USA **107**, 21311 (2010).

[21] D. K. Yoon, Y. Yi, Y. Shen, E. D. Korblova, D. M. Walba, I. I. Smalyukh, and N. A. Clark, Adv. Mater. **23**, 1962 (2011).

[22] T. Gong, Ph.D. thesis, University of Colorado, 2011.

[23] See Supplemental Material at http://link.aps.org/supplemental/10.1103/PhysRevE.89.032502 for the synthetic procedure of the material, depolarized reflection light microscopy images, and grazing incidence x-ray diffraction data.

[24] R. A. Reddy, C. Zhu, R. Shao, E. Korblova, T. Gong, Y. Shen, E. Garcia, M. A. Glaser, J. E. Maclennan, D. M. Walba, and N. A. Clark, Science **332**, 72 (2011).

[25] S. Grigoras and T. H. Lane, J. Comput. Chem. **8**, 84 (1987).

[26] S. Grigoras and T. H. Lane, J. Comput. Chem. **9**, 25 (1988).

[27] J. Naciri, J. Ruth, G. Crawford, R. Shashidhar, and B. R. Ratna, Chem. Mater. **7**, 1397 (1995).

[28] J. B. Foumier and G. Durand, J. Phys. II **1**, 845 (1991).

[29] M. Kleman and O. D. Lavrentovich, Liq. Cryst. **36**, 1085 (2009).

[30] Y. H. Kim, D. K. Yoon, H. S. Jeong, O. D. Lavrentovich, and H.-T. Jung, Adv. Funct. Mater. **21**, 610 (2011).

[31] Y. H. Kim, D. K. Yoon, H. S. Jeong, and H.-T. Jung, Soft Matter **6**, 1426 (2010).

[32] L. He, Z. X. Shen, Z. Yin, M. S. Zhang, and S. H. Tang, Liq. Cryst. **26**, 63 (1999).

[33] B. Lee, I. Park, J. Yoon, S. Park, J. Kim, K.-W. Kim, T. Chang, and M. Ree, Macromolecules **38**, 4311 (2005).

[34] Y. Shen, L. Wang, R. Shao, T. Gong, C. Zhu, H. Yang, J. E. Maclennan, D. M. Walba, and N. A. Clark, Phys. Rev. E **88**, 062504 (2013).

[35] M. Ibn-Elhaj, A. Skoulios, D. Guillon, J. Newton, P. Hodge, and H. J. Coles, J. Phys. II **6**, 271 (1996).

[36] A. de Vries, Mol. Cryst. Liq. Cryst. **10**, 31 (1970).

[37] A. de Vries, Mol. Cryst. Liq. Cryst. **10**, 219 (1970).

[38] L. V. Azaroff, Proc. Natl. Acad. Sci. USA **77**, 1252 (1980).

[39] M. Nagaraj, A. Lehmann, M. Prehm, C. Tschierske, and J. K. Vij, J. Mater. Chem. **21**, 17098 (2011).